Numerical Analysis of Hybrid Cooling Impacts on Battery Temperature under High Discharge and Outdoor Conditions

Sena Abraham Irsyad[1], *Alief* Wikarta[1*], and *Is* Bunyamin Suryo[1]

[1]Institut Teknolgi Sepuluh Nopember, Mechanical Engineering Department, Jalan Arif Rahman Hakim, Keputih – Sukolilio, Surabaya 60111, Jawa Timur Indonesia

Abstract. As the demand for renewable energy grows and environmental consciousness increases, there's a rising interest in electric devices as environmentally friendly solutions. However, lithium-ion batteries used in these devices are susceptible to temperature increases, particularly in outdoor settings, which can impact their performance. To tackle this issue, hybrid cooling systems that combine water cooling and PCM technology are being explored to optimize efficiency outdoors. This study aims to examine how well hybrid cooling systems perform in controlling battery temperature under two operational conditions: changes in speed and working fluid temperature. The speeds used are 0.075 L/min, 0.15 L/min, 0.3 L/min, 0.45 L/min, 0.6 L/min, and 0.75 L/min with water temperatures of 20°C, 25°C, 27°C, and 29°C at discharge rates of 1C and 2C. Results indicate that for a 1C discharge, cooling is effective at a speed of 0.15 L/min with a working temperature of 29°C, as the battery temperature remains below its maximum operational threshold. However, for a 2C discharge, the optimal condition is a flow temperature of 25°C with a speed of 0.6 L/min. Therefore, the proposed conditions can ensure that the battery temperature remains within a safe operating limit.

1 Introduction

With a significant reliance on fossil fuels, there has been heightened attention on global energy and environmental issues in recent decades [1]. Vehicles equipped with internal combustion engines consume higher amounts of fuel and are acknowledged as major sources of pollution [2]. As an optimal solution, the adoption of electric vehicles serves to address energy challenges while reducing carbon emissions and pollution. Lithium-ion (Li-ion) batteries stand out as highly popular energy storage mediums today [3]. In practical application and placement, battery packs are typically situated in two distinct environmental conditions there are enclosed spaces and open areas. However, the performance of lithium-ion batteries suffers when temperatures fall outside the suitable range [4]. This thermal challenge predominantly arises due to the low thermal conductivity of lithium batteries,

* Corresponding author: wikarta@me.Its.ac.id

leading to significant temperature spikes during high-load operations [5]. Extreme temperature increases in lithium-ion batteries can trigger internal decomposition reactions, posing potential risks of battery explosions [6].

Excessive temperature challenges can be tackled by integrating a cooling system into the battery pack. In describing the heat generation rate to illustrate battery heat growth phenomena, the Bernardi equations are still utilized [7]. With a steady input heat generation rate, numerous studies have explored battery cooling methods, spanning from cell-level models to storage. Beginning with passive cooling strategies, active cooling, to the amalgamation of both termed hybrid cooling [8]. Incorporating fans as a means of forced cooling to enhance heat transfer from the battery, constitutes one of the active air cooling methods [9]. Despite its tendency towards inefficiency, air cooling can be optimized by identifying suitable inlet and outlet positions [10]. Moreover, passive cooling approaches leverage Phase Change Material (PCM) and hydrogel to absorb battery cell-generated heat, with adequate spacing between cells serving as a viable solution [11]. The application of thermoelectric cooling to lithium batteries may involve employing thermoelectric modules or materials surrounding the battery [12].

Merging both cooling methodologies often termed as hybrid cooling, stands as an ongoing endeavor aimed at augmenting the efficiency of battery cooling systems. The adoption of hybrid cooling holds promise in delivering superior performance by addressing the shortcomings inherent in individual cooling methods [13]. The integration of two cooling systems, such as liquid cooling with materials like silica that exhibit properties resembling PCM, is one approach [14]. Furthermore, PCM boasts a notable latent heat capacity, facilitating heat absorption or dissipation during phase transitions [15]. Alternate combinations encompass the fusion of water cooling with PCM, alongside PCM integration with heat pipe technology [16]. Exploration into PCM and liquid cooling system amalgamation spans diverse channel designs, flow parameters, and control strategies [17]. The efficacy of battery cooling is influenced by the number of cooling channels employed, surpassing the optimal threshold and offering minimal additional benefits [18].

The primary goal of this study is to offer a reliable depiction of an effective hybrid cooling system suitable for outdoor use. The research aims to achieve optimal battery operation under specific conditions, ensuring that cooling methods maintain the battery temperature within the ideal range. This hybrid cooling approach combines both active and passive cooling techniques. Active cooling involves circulating water through an aluminum pipe positioned among the battery cells, while passive cooling utilizes PCM materials to fill the empty spaces between cells not occupied by the aluminum pipe. Furthermore, the study will explore how varying the time step size affects the representation of battery pack heat growth behavior.

2 Simulation Method

2.1 Domain Modelling

The research utilizes a battery cell configuration comprising 16 cells. Each cell has a maximum capacity of 100 Ah and a nominal voltage of 3.2 Volts. The layout of the battery cells forming the pack with hybrid cooling is depicted in Figure 1(a), where each cell measures 36.7 mm in width (z), 130.5 mm in height (y), and 195.5 mm in length (x). Simplification was employed as a solution to reduce computational time.

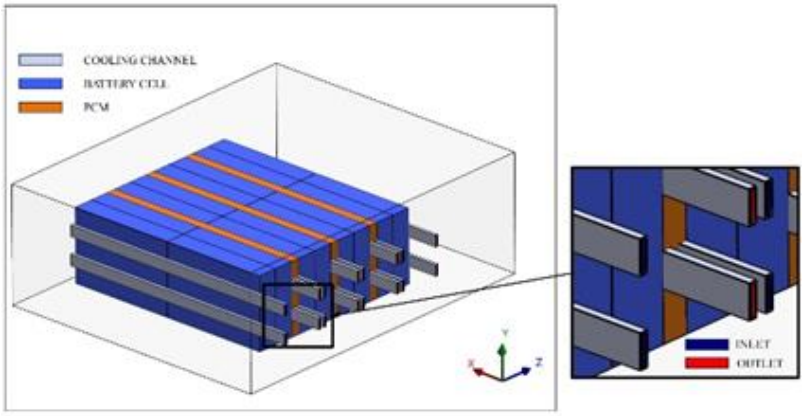

Fig. 1 Illustrates battery pack domain employing hybrid cooling

2.2 Set-up and Processing

The entire surface of the pack casing is designated as a wall with a constant convection heat transfer coefficient of 10 W/m2. The convergence criterion is set at a residual value of 10^{-4} with a maximum of 150 iterations per time step. A laminar viscous model is employed [19], with an initial condition of T = 27°C for the battery and a SIMPLE scheme. The calculation of the heat generation rate utilizes the Bernardi equations [7], as shown in equations 1 and 2, where the values depend on the volume (V) of the battery cell and the power (Q) produced from the discharge process. The value of dOCV/dT follows the reference of 0.5 mV/K [20], resulting in a heat generation rate of 22381 W/m^3 for 1C and 52630 W/m^3 for 2C discharge rates. The heat source is applied to the battery cell with a constant heat generation rate throughout its volume. The process of PCM melting is neglected to simplify the heat transfer model [21].

$$q'''= Q/V \quad (1)$$

$$Q=I[IR+T\,\partial OCV/(\partial Ta)] \quad (2)$$

The mixture boundary conditions are utilized to define the surrounding conditions. Combining radiation and convection is appropriate for approximating outdoor modeling. These boundary conditions will be applied to all walls except the bottom wall because of the assumption that the pack is placed on another surface. Hence, the bottom wall surface will be considered to have a boundary condition of heat flux = 0. The fluid used for hybrid cooling is water. In addition to the working fluid, there are aluminum pipes through which the working fluid flows, as well as PCM materials. Table 1 below displays the properties of the solid material used in the hybrid cooling simulation.

Table 1. The solid properties of the materials.

Parameter	Aluminium	PCM	Battery Cell
Density	2700 kg/m³ [19]	950 kg/m³ [21]	1700 kg/m³ [19]
Thermal Conductivity	238 W/m.K [19]	7.654 W/m.K [21]	34 W/mK(x and y), 8.2 W/mK (z) [22]
Spesific Heat Capacity	900 J/kg.K [19]	3000 J/kg.K [21]	830 J/kg.K [19]

The size of the cooling pipes used is also one of the fixed parameters of hybrid cooling, similar to that studied by Lan (2016) [19] with hole dimensions of 3 mm x 3 mm, totaling 4 holes per pipe used. In this study, it will be simplified to a single hole with dimensions of 3 mm x 18 mm. The length of the pipe follows the perimeter size of the battery configuration illustrated in Figure 2, which consists of 4 cells. In addition to the discharge rate used, this study will also vary the conditions of inlet flow velocity and temperature. The velocities used are 0.075 L/min, 0.15 L/min, 0.3 L/min, 0.45 L/min, 0.6 L/min, and 0.75 L/min. The working temperature at each velocity is 20°C, 25°C, 27°C, and 29°C

2.3 Grid Independency Test and Validation

A grid independence test was conducted using mesh counts ranging from 1 million to 4 million elements. The results of this grid independence test were obtained by considering the maximum temperature extracted from two different domains. The criterion used for evaluation was the maximum temperature of the battery and working fluid. The relative error percentages obtained were all below 1%. Therefore, the decision to use a mesh with 2 million elements was deemed appropriate. This decision was made under the assumption that, with this mesh element count, the heat transfer phenomena are adequately represented.

Validation was conducted by comparing the simulation setup with previous research. In the study by Lan et al. (2016) , simulations were performed with several numbers of cooling channels. The maximum temperature obtained by Lan et al. (2016) under the conditions of an inlet velocity boundary of 0.05 L/min and a fluid temperature of 27°C was 29.35°C. The simulation was conducted with fine meshing consisting of 418.192 elements. When replicating the setup under the same boundary conditions, the obtained temperature was 29.48°C. The validation simulation used meshing with a total of 418.680 elements. The difference in results between the two simulations was less than 1%, indicating that the simulation can be used with the applied setup, despite changes in materials and other parameter values.

3 Result and Discussion

After completing the initial procedures, including grid independence and validation, the next step involves analyzing the influence of variations in flow velocity and fluid temperature on the battery temperature distribution. This analysis will be conducted for each discharge rate used: 1C, 2C, and 3C. Table 2 below will present the simulation results in the form of a summary of maximum temperatures under all conditions utilized.

Table 2. Summary of maximum temperatures.

No	Discharge Rate (C)	Flow rate inlet (L/min)	Max Battery Cell Temperature at Inlet Temperature Variation (ºC)			
			29ºC	27 ºC	25 ºC	20 ºC
1	1	0.075	43.62	41.68	39.73	34.87
2		0.15	38.66	36.67	34.68	29.72
3		0.3	36.39	34.40	32.40	27.44
4		0.45	35.64	33.64	31.65	26.69
5		0.6	35.24	33.24	31.25	26.29
6		0.75	34.98	32.99	31.00	26.03

7	**2**	**0.075**	59.29	57.69	56.10	52.11
8		**0.15**	50.87	48.99	47.10	42.40
9		**0.3**	46.17	44.21	42.25	37.35
10		**0.45**	44.50	42.53	40.55	35.61
11		**0.6**	43.60	41.62	39.64	34.68
12		**0.75**	43.03	41.04	39.06	34.10

3.1 The Effect of Changes in Speed and Temperature of the Working Fluid on a 1C Discharge Rate

The results obtained for the 1C discharge rate are depicted in the graph shown in Figure 2 below. In Figure 2(a), where the working fluid temperature is 29°C, there is a significant decrease in the maximum battery temperature across the range of inlet velocities from 0.075 L/min to 0.45 L/min. At a velocity of 0.075 L/min and a flow temperature of 29°C, the maximum battery temperature is recorded at 43.62°C. Comparing this with the maximum battery temperature obtained at a velocity of 0.15 L/min and the same flow temperature, there is a decrease of approximately 11%. Similarly, comparing it with the condition at a flow rate of 0.45 L/min, there is a decrease of around 18%. The increase achieved is only about 6% by increasing the velocity up to six times faster than before. However, for a 1C discharge rate condition, there is no need to increase the flow velocity beyond 0.15 L/min at a working temperature of 29°C. This is because the maximum battery temperature obtained is already below 40°C, indicating it is within the safe range for battery operation.

The results obtained do not differ significantly when comparing the outcomes in Figure 2(b) with the previous condition. In this scenario as well, the maximum battery temperature at the end of discharge with a flow velocity of 0.15 L/min is already below the safe limit. Comparing the two flow temperature conditions at this velocity, namely 29°C and 27°C, yields a difference of approximately 5%. The values obtained for this comparison are not significant. Similarly, the increase in maximum battery temperature at flow velocities above 0.15 L/min under these two flow temperature conditions is less than 2%.

However, examining the results under the flow temperature conditions of 25°C and 20°C as shown in Figures 2(c) and (d) reveals different outcomes. At the lowest flow velocity of 0.075 L/min, the maximum battery temperature is already below the safe operating limit. This result is quite different compared to the two previous flow temperature conditions. Comparing the maximum battery temperature obtained under the flow temperature conditions of 29°C and 20°C at the lowest velocity yields a difference of up to 20%. This figure is quite significant compared to the differences obtained from previous comparisons. However, if environmental conditions only permit the use of a working fluid with a temperature of 29°C, the solution offered is to increase the flow velocity to 0.15 L/min. However, if conditions allow for adjusting the temperature of the flowing fluid, simply reducing it to 25°C with a flow velocity of 0.075 L/min will suffice.

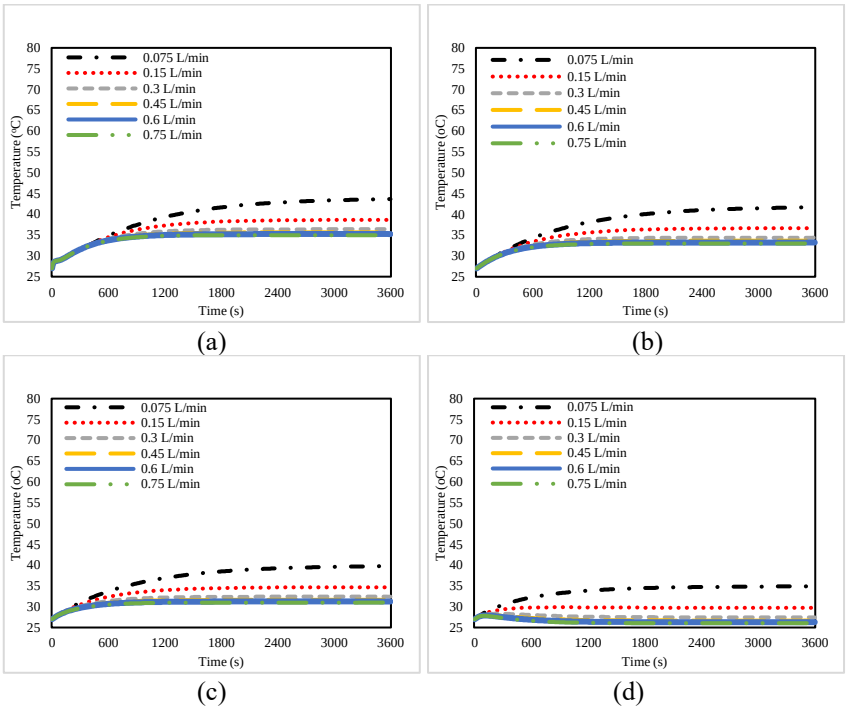

Fig. 2 Graph of temperature rise during discharge at a 1C rate at working fluid temperatures of (a) 29°C, (b) 27°C, (c) 25°C, and (d) 20°C.

In Figure 3, the temperature contours on the battery pack under the flow temperature condition of 29°C with all velocities used will be visualized. It can be observed that the heat distribution on the battery tends to be higher on the side closer to the outlet and does not come into contact with the PCM. However, as the velocity increases, the heat distribution tends to become more uniform. Nevertheless, the heat distribution on the battery at a velocity of 0.15 L/min has already started to become uniform. Although it tends to be hotter on one side, it is already within the safe limits of the optimal maximum battery operational temperature. However, upon observing Figure 2(d), the highest speed used resulted in a maximum battery temperature of approximately 45.05°C. This value differs by about 5.05°C or equivalent to 11% when compared to the safe battery temperature limit. Under the same speed conditions, with a flow temperature of 25°C, the maximum battery temperature reached 49.88°C. This yields a difference of about 4.83°C or approximately 10% when compared to the results obtained under a flow temperature of 20°C for the maximum speed used in this study. Therefore, the proposed cooling conditions are not effective in limiting the rise in battery temperature during a 3C discharge.

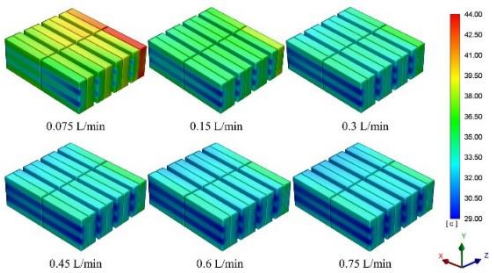

Fig. 3 The temperature contour visualization during a 1C discharge with a fluid flow temperature of 29°C across all speed variations.

3.2 The Effect of Changes in Speed and Temperature of the Working Fluid on a 2C Discharge Rate

For the 2C discharge rate, the results differ significantly from the previous 1C discharge. The outcomes obtained for the 2C discharge rate are depicted in the graph shown in Figure 4 below. At the lowest flow velocity under all temperature conditions used, a relatively high maximum battery temperature is obtained. At a flow temperature of 29°C, the maximum temperature obtained is 59.29°C, compared to the lowest flow temperature condition which yields a temperature of 52.11°C at a velocity of 0.075 L/min, resulting in a difference of up to 12%. This is in stark contrast to the results for the 1C discharge, which showed differences of up to 20% under the same conditions.

Upon examining the graphs presented in Figures 4(a) and (b), it's evident that the increase in maximum battery temperature is still not within the optimal battery usage range. However, under the flow temperature conditions of 25°C and 20°C, as depicted in Figures 4(c) and (d), specific velocities can potentially lower the battery temperature to the maximum allowable limit. For instance, under the 25°C flow temperature condition, elevating the flow velocity eightfold compared to the lowest velocity results in a maximum battery temperature of 39.64°C. Conversely, at the lowest flow temperature condition, a maximum temperature of 37.35°C is attained at a velocity of 0.3 L/min, which is half that of the 25°C flow temperature condition. When comparing both scenarios at the same velocity of 0.3 L/min with a fluid temperature of 25°C, the maximum battery temperature reaches 42.25°C. This comparison reveals a percentage difference of up to 12%.

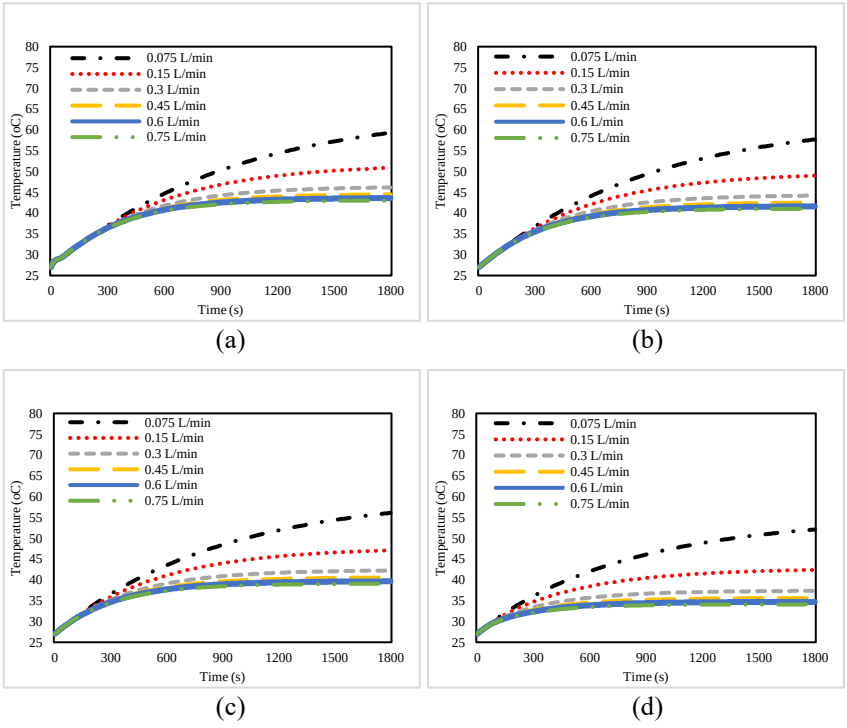

Fig. 4 Graph of temperature rise during discharge at a 2C rate at working fluid temperatures of (a) 29°C, (b) 27°C, (c) 25°C, and (d) 20°C

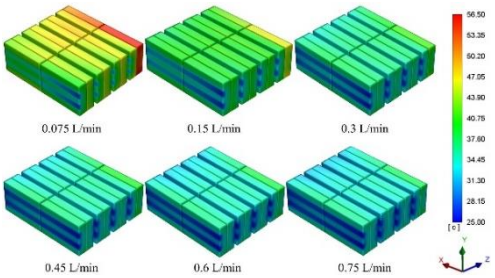

Fig. 5 The temperature contour visualization during a 2C discharge with a fluid flow temperature of 25°C across all speed variations.

In deciding the preferable condition, it's advisable to initially assess the environmental circumstances. If environmental conditions only allow for the use of a working fluid at 25°C, the recommended solution is to increase the flow velocity to 0.6 L/min. However, if conditions permit altering the temperature of the flowing fluid, then it's necessary to decrease it to 20°C with a flow velocity of 0.3 L/min. Figure 5 will visualize temperature contours on the battery pack under the flow temperature condition of 25°C with all velocities used, considering a 2C discharge rate. The visual depiction doesn't differ significantly from what was obtained under the 1C discharge condition. Heat accumulation predominantly occurs on one side near the outlet and doesn't come into contact with the PCM.

4 Conclusion

Based on the results obtained and the discussion above, the following conclusions can be drawn:

1. Flow conditions at a speed of 0.075 L/min with a temperature of 25°C can lower the maximum battery temperature during a 1C discharge to below 40°C. Additionally, doubling the speed can provide a decrease in the maximum battery temperature below the safety limit at a flow temperature of 29°C. These two outcomes would serve as alternative solutions for potential outdoor conditions during a 1C discharge.
2. For a 2C discharge, it is necessary to increase the speed to 0.6 L/min with a flow temperature of 25°C to achieve a maximum battery temperature below the safety limit. Another solution offered is to lower the flow temperature to 20°C, thus requiring only half the flow speed of the previous solution.

References

1. K. Whiting, L. G. Carmona, and T. Sousa, “A review of the use of exergy to evaluate the sustainability of fossil fuels and non-fuel mineral depletion,” Renewable and Sustainable Energy Reviews, vol. 76. Elsevier Ltd, pp. 202–211, (2017). doi: 10.1016/j.rser.2017.03.059.
2. V. Etacheri, R. Marom, R. Elazari, G. Salitra, and D. Aurbach, “Challenges in the development of advanced Li-ion batteries: A review,” Energy and Environmental Science, vol. 4, no. 9. pp. 3243–3262, Sep. (2011). doi: 10.1039/c1ee01598b.
3. A. D. Bank, Handbook on Battery Energy Storage System. Manila, Philippines: Asian Development Bank, (2018). doi: 10.22617/TCS189791-2.
4. Z. Ling, F. Wang, X. Fang, X. Gao, and Z. Zhang, “A hybrid thermal management system for lithium ion batteries combining phase change materials with forced-air cooling,” Appl Energy, vol. 148, pp. 403–409, Jun. (2015), doi: 10.1016/j.apenergy.2015.03.080.

5. D. Deng, Li-ion batteries: Basics, progress, and challenges, vol. 3, no. 5. John Wiley and Sons Ltd, (2015). doi: 10.1002/ese3.95.
6. S. Mallick and D. Gayen, "Thermal behaviour and thermal runaway propagation in lithium-ion battery systems – A critical review," Journal of Energy Storage, vol. 62. Elsevier Ltd, Jun. 01, (2023). doi: 10.1016/j.est.2023.106894.
7. D. Bernardi, E. Pawlikowski, and J. Newman, "A GENERAL ENERGY BALANCE FOR BATTERY SYSTEMS," Soc. vol. 132, no. 1, pp. 5-12, (1985)
8. J. R. Patel and M. K. Rathod, "Recent developments in the passive and hybrid thermal management techniques of lithium-ion batteries," Journal of Power Sources, vol. 480. Elsevier B.V., Dec. 31, (2020). doi: 10.1016/j.jpowsour.2020.228820.
9. M. Akbarzadeh et al., "A comparative study between air cooling and liquid cooling thermal management systems for a high-energy lithium-ion battery module," Appl Therm Eng, vol. 198, Nov. (2021), doi: 10.1016/j.applthermaleng.2021.117503.
10. Y. Yang, X. Xu, Y. Zhang, H. Hu, and C. Li, "Synergy analysis on the heat dissipation performance of a battery pack under air cooling," Springer-Verlag GmbH Germany, (2020), doi: 10.1007/s11581-020-03676-5/Published.
11. M. M. Khan, M. Alkhedher, M. Ramadan, and M. Ghazal, "Hybrid PCM-based thermal management for lithium-ion batteries: Trends and challenges," J Energy Storage, vol. 73, p. 108775, Dec. (2023), doi: 10.1016/j.est.2023.108775.
12. H. Sait, "Cooling a plate lithium-ion battery using a thermoelectric system and evaluating the geometrical impact on the performance of heatsink connected to the system," J Energy Storage, vol. 52, Aug. (2022), doi: 10.1016/j.est.2022.104692.
13. X. Xu, X. Chen, J. Shen, J. Kong, H. Zhang, and F. Zhou, "Thermal management system for prismatic battery module with biomimetic cephalofoil fin and film heater," Appl Therm Eng, vol. 227, Jun. (2023), doi: 10.1016/j.applthermaleng.2023.120379.
14. Z. Liu, M. Cao, Y. Zhang, J. Li, G. Jiang, and H. Shi, "Thermal management of cylindrical battery pack based on a combination of silica gel composite phase change material and copper tube liquid cooling," J Energy Storage, vol. 71, Nov. (2023), doi: 10.1016/j.est.2023.108205.
15. Z. Zhou et al., "Experimental study on the thermal management performance of phase change material module for the large format prismatic lithium-ion battery," Energy, vol. 238, Jan. (2022), doi: 10.1016/j.energy.2021.122081.
16. Z. Leng, Y. Yuan, X. Cao, C. Zeng, W. Zhong, and B. Gao, "Heat pipe/phase change material thermal management of Li-ion power battery packs: A numerical study on coupled heat transfer performance," Energy, vol. 240, Feb. (2022), doi: 10.1016/j.energy.2021.122754.
17. G. Wu, F. Liu, S. Li, N. Luo, Z. Liu, and Y. Li, "Research on Performance Optimization of Liquid Cooling and Composite Phase Change Material Coupling Cooling Thermal Management System for Vehicle Power Battery," J Renew Mater, vol. 11, no. 2, pp. 707–730, (2023), doi: 10.32604/jrm.2022.022276.
18. C. Wang et al., "Liquid cooling based on thermal silica plate for battery thermal management system," Int J Energy Res, vol. 41, no. 15, pp. 2468–2479, Dec. (2017), doi: 10.1002/er.3801.
19. C. Lan, J. Xu, Y. Qiao, and Y. Ma, "Thermal management for high power lithium-ion battery by minichannel aluminum tubes," Appl Therm Eng, vol. 101, pp. 284–292, May (2016), doi: 10.1016/j.applthermaleng.2016.02.070.

20. W. Li, X. Zhuang, and X. Xu, “Numerical study of a novel battery thermal management system for a prismatic Li-ion battery module,” in Energy Procedia, Elsevier Ltd, (2019), pp. 4441–4446. doi: 10.1016/j.egypro.2019.01.771.
21. K. Chen, J. Hou, M. Song, S. Wang, W. Wu, and Y. Zhang, “Design of battery thermal management system based on phase change material and heat pipe,” Appl Therm Eng, vol. 188, Apr. (2021), doi: 10.1016/j.applthermaleng.2021.116665.
22. K. C. Chiu, C. H. Lin, S. F. Yeh, Y. H. Lin, and K. C. Chen, “An electrochemical modeling of lithium-ion battery nail penetration,” J Power Sources, vol. 251, pp. 254–263, Apr. (2014), doi: 10.1016/j.jpowsour.2013.11.069.